Tribology Letters (2018) 66:18
https://doi.org/10.1007/s11249-017-0961-2

ORIGINAL PAPER

The Influence of Cu/Fe Ratio on the Tribological Behavior of Brake Friction Materials

Tao Peng[1] · Qingzhi Yan[1] · Gen Li[2] · Xiaolu Zhang[1]

Received: 20 June 2017 / Accepted: 21 November 2017 / Published online: 8 December 2017

Abstract
Copper and iron are the major ingredients in friction materials, among which Fe often been served as friction reinforcement in the past. But in our recent study, the coefficients of friction (COF) decreased with increasing iron content in composites. In order to study the influence of Cu/Fe ratio on the tribological behavior of the composite under simulative braking conditions, a subscale testing apparatus with the pad-on-disk configuration under various initial braking speeds (IBS) was applied. The changes in mean COFs, wear rates, morphologies and chemical constitutions of friction surface for different composites were investigated. Results showed that the composite containing more Fe content always showed lower mean COF and wear rate, which different from the previous studies. This is because, under severe braking conditions, the tribological behavior of composite mainly depends on the evolution of tribo-oxide film on the surface, not just on the substrate themselves. Higher Fe content accelerated the formation of tribo-oxide film and in turn inhibited the destruction of tribo-oxide film on the surface, which leading to lower mean COF and wear rate, as well as a higher critical IBS for the transition of mean COF and wear rate. This work also provides a way to characterize the fracture strength of tribo-film by carried out a peeling test.

Keywords Brake friction material · Subscale test · Tribo-oxide film · Tribological behavior

1 Introduction

Friction materials prepared by powder metallurgy technique with various powder ingredients have been developed widely for application in many industrial areas, such as brakes and clutches [1–3], due to their energy absorption capacity, thermotolerance and low wear rate [4, 5]. Meanwhile, it is easy to control the friction by changing the composition of the powdered metals especially for unlubricated sliding [6, 7].

Copper and iron have been widely applied to the friction materials by virtue of their lower prices and desirable mechanical properties [3, 8–10]. There are many studies carried on the tribological performance of the composites containing the two ingredients [2, 6, 7, 11–14]. Many researchers found that the increase in Fe content often led to the increase in the friction coefficient, and sometimes was responsible for the decrease in the wear loss. Hence, Fe was often seen as reinforcement in the past [1, 6], which plays roles in enhancing friction and alleviating wear of composites.

Xiong et al. [6] studied the effect of Fe on the tribological properties of Cu-based friction materials against 30CrMoSiVA steel using a ring-on-disk method, with sliding speeds in the range of 3–24 m/s at a pressure of 0.5 MPa and a rotary inertia of 0.245 kg m^2. The fabrication of sample in their work was based on keeping parent composition of some ingredients (9 wt%) constant and varying Cu and Fe in a complementary manner. They reported the friction coefficient increased with the increase in Fe content from 0 to 12 wt%, and attributed this result to the properties of Fe itself, i.e., (1) Fe enhanced the engaging force between the mating surfaces due to its higher strength and hardness than that of Cu; (2) Fe had a better adhesive force to the mating steel than Cu due to its better compatibility with steel.

However, these studies merely conducted under mild sliding conditions (lower applied pressure or lower sliding speed or lower rotary inertia) [1, 6], which far from the realistic

✉ Qingzhi Yan
qzyan@ustb.edu.cn

[1] Laboratory of Special Ceramics and Powder Metallurgy, University of Science and Technology Beijing, Beijing 100083, China

[2] Division of Surface and Corrosion Science, Department of Chemistry, KTH Royal Institute of Technology, 10044 Stockholm, Sweden

condition of brake friction materials. Furthermore, the tribo-oxidation is inevitable under real braking, and the metals mainly exist in the form of oxides on the friction surface [15, 16]. These produced oxides and many other particles then were transformed into wear debris, which will be further compacted and sintered to form third body layer (also called tribo-film, friction layer, etc.) on the friction surface [17, 18]. Therefore, the role of metal on the tribological performance of the composites may virtually depend on the produced tribo-oxide film within the contact zone.

Currently, it is widely believed that the tribo-oxide film play roles in separating the other two bodies and preventing metal-on-metal contact, contributing to a stable friction and low wear regime as long as it is not destroyed [19–23]. Recently, we also found the close relevance between the tribological behaviors and friction film [24], in which the decrease in mean COF and wear rate regularly corresponding to the formation and completion of friction film due to its coverage on the metal surface and hard particles, while the increase in mean COF and wear rate corresponding to the non-formation or destruction of friction film. And similar relevance already was demonstrated by Huang et al. [25] in another tribology system. Therefore, the tribological behaviors of the composite should be more correlated with the formation and destruction of tribo-oxide film than the substrate themselves.

The objectives of the work were to study the influence of Cu/Fe ratio on the tribological behavior of the composites under simulative braking conditions, and the relationship between Cu/Fe ratio and the formation of tribo-oxide film also were revealed. The friction tests were carried out on a subscale testing apparatus with the pad-on-disk configuration under different unlubricated conditions. For different samples, the mean COFs, wear rates, and fracture strengths of tribo-oxide film at various IBS were investigated as well as the morphologies by means of scanning electron microscopy and energy-dispersive spectroscopy analysis.

2 Experiments

2.1 Sample

The fabrication of samples containing Cu (4–7 μm, 99.5% pure), Fe (10–18 μm, 99% pure), graphite (250–500 μm, 97% pure), Cr (10–23 μm, 99.5% pure), ferrochrome alloy (Cr–Fe) (120–250 μm, 98% pure), MoS_2 (18–48 μm, 99% pure), SiO_2 (58–120 μm, 99% pure), binder, etc., was based on keeping parent composition of some ingredients (32 wt%) constant and varying two ingredients, i.e., Cu and Fe in a complementary manner to ensure the ratio of Cu/Fe decrease proportionately (Table 1). The ingredients (except graphite powder) were firstly mixed up in a *V*-type blender for 1.5 h and then mixed with graphite powder for additional 0.5 h. The mixed powders were then pressed into green bodies under a pressure of 300 MPa in a steel mold. The green bodies were then sintering at 980 °C in a controlled atmosphere furnace. Figure 1 shows the backscattered electron image (BSE) of sintered samples, in which some of the components are indicated based on the energy-dispersive X-ray spectrometry (EDS) identification. Note that some components, like graphite, Cr–Fe particles, and SiO_2, preserve the original powder appearances. The nominal contact surface of the braking pads was 1787 mm^2. A forged steel rotor disk (30CrSiMoVA) with a diameter of 450 mm and a thickness of 35 mm was applied as a counterface, which is widely assembled in current high-speed train in China.

2.2 Friction Tests

The friction tests were carried out on a subscale testing apparatus (TM-I, China, Fig. 2) under the ambient temperature of 30 °C and the relative humidity of 40% in the pad-on-disk configuration, more details about the tester can be found in [24]. In order to compare the tribological behaviors of different samples under different speeds, four representative initial braking speeds (IBS), varying from 12 to 60 m/s (12, 31, 47, 60 m/s), corresponding to 80–380 km/h for the train, were selected. The braking inertia was set as 27 kg m^2 corresponding to 17.2 tons of mass to be stopped per disk in the real train based on a scale-conversion rule [26], and the normal pressure was 1.1 MPa corresponding to an emergency braking event.

During each test, the braking disk was equipped as a rotator of the test machine and driven by an AC motor to a certain rotating speed, i.e., the IBS. Then, two fixed braking pads, equipped as the stators of the machine, were pressed to the braking disk simultaneously, resulting in a mean friction radius of 125 mm and a nominal contact area of 1787 mm^2. When the rotator reached the set speed, it was cut off from

Table 1 Compositions of the samples (by wt%)

Sample	Cu	Fe	Cr–Fe	Graphite	MoS_2	SiO_2	Others	Ratio of Cu/Fe
S1	60	8	8.0	10	2.5	5.0	6.5	7.5
S2	48	20						2.4
S3	30	38						0.79
S4	14	54						0.26

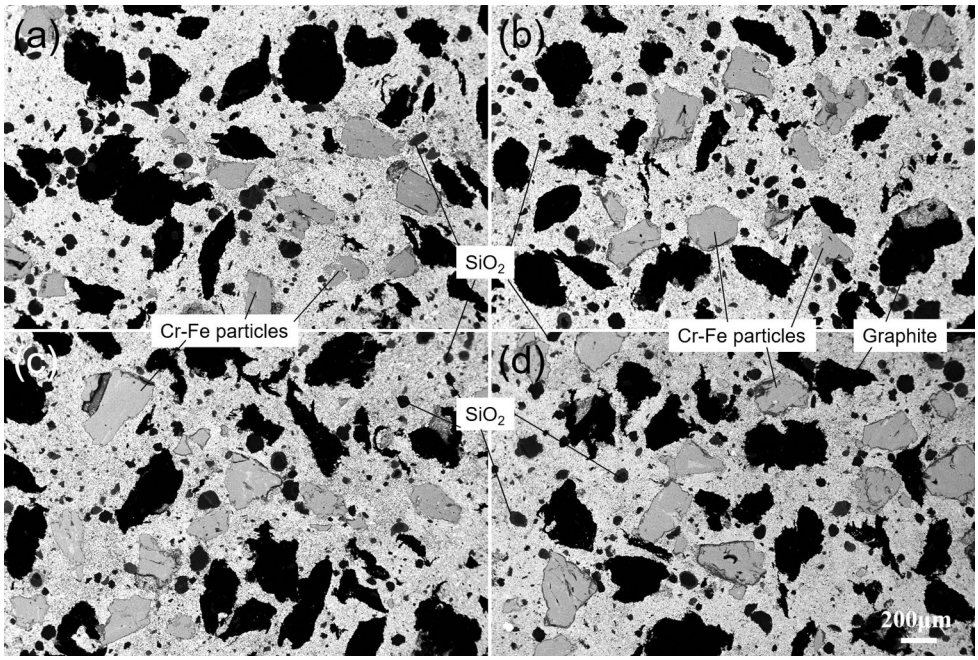

Fig. 1 Backscattered electron image (BSE) of starting samples. **a** S1, **b** S2, **c** S3, **d** S4. The bar scale is same for all the images

the motor, and slowed down consequently due to the drag of pad friction. Then, the mean COF, μ_t, was automatically calculated by the computer system based on Eq. (1):

$$\mu_t = \frac{\int_0^{t_s} \mu \mathrm{d}t}{t_s} \tag{1}$$

where μ is the transient COF and t_s is the stopping time. The wear rate, W_r, of the pad samples was determined by measuring their weights before and after testing in an analytical balance (D&T ES5000, with an accuracy of 0.01 g). The W_r was calculated by normalizing the weight loss by the total sliding distance, S, using Eq. (2):

$$W_r = \Delta M / S \tag{2}$$

The bulk temperature of the pad was measured by a thermocouple located 2 mm beneath the contact surface within the pad. Before each test, we conducted seven times run-in brakes with an initial braking speed of 25 m/s and a normal pressure of 1.1 MPa to ensure a favorable contacting surface between the pad and disk. To ensuring the reliability of the experiment's data, the braking test at each speed was repeated three times and the mean value (mean COF, mean wear loss) of three is reported in this work.

2.3 Characterization Methods

The density and porosity were tested via Archimedes' principle. The Brinell hardness of the initial samples was tested on the HB-3000 hardness tester (China) in accordance with GB/T 231.1-2009. The shear strength was measured on the WDT-20 universal testing machine (China) based on TJ/CL 307-2014.

Scanning electronic microscope (SEM, ZEISS, LEO1450, Germany) attached with energy-dispersive X-ray spectrometry (EDS, OXFORD, 51-XMX, UK) was applied to examine the surface morphologies of the friction pads after the friction tests. X-ray diffraction (XRD, RIGAKU, SmartLab, Japan) measurements were taken to identify the crystalline phases in the friction surface. Laser confocal microscopy (LCM, OLYMPUS, OLS4100, Japan) was used to measure the surface roughness (R_a) of the friction surface.

3 Results

3.1 Physical and Mechanical Properties

Table 2 shows physical and mechanical properties, including porosity, density, Brinell hardness, and shear strength of the samples in this investigation. The porosities of the samples were nearly identical, which may be because graphite particles as well as the graphite/metals boundaries were the main source of pores and the identical graphite contents for all the samples. The decrease in densities with the increase in Fe content can be attributed to the lower theoretical density of Fe. Although Fe has better mechanical strength than that of Cu, the sintering temperature was insufficient for the sample contain more Fe, and it was responsible for only slight increases of the Brinell hardness and the shear strength with Fe content.

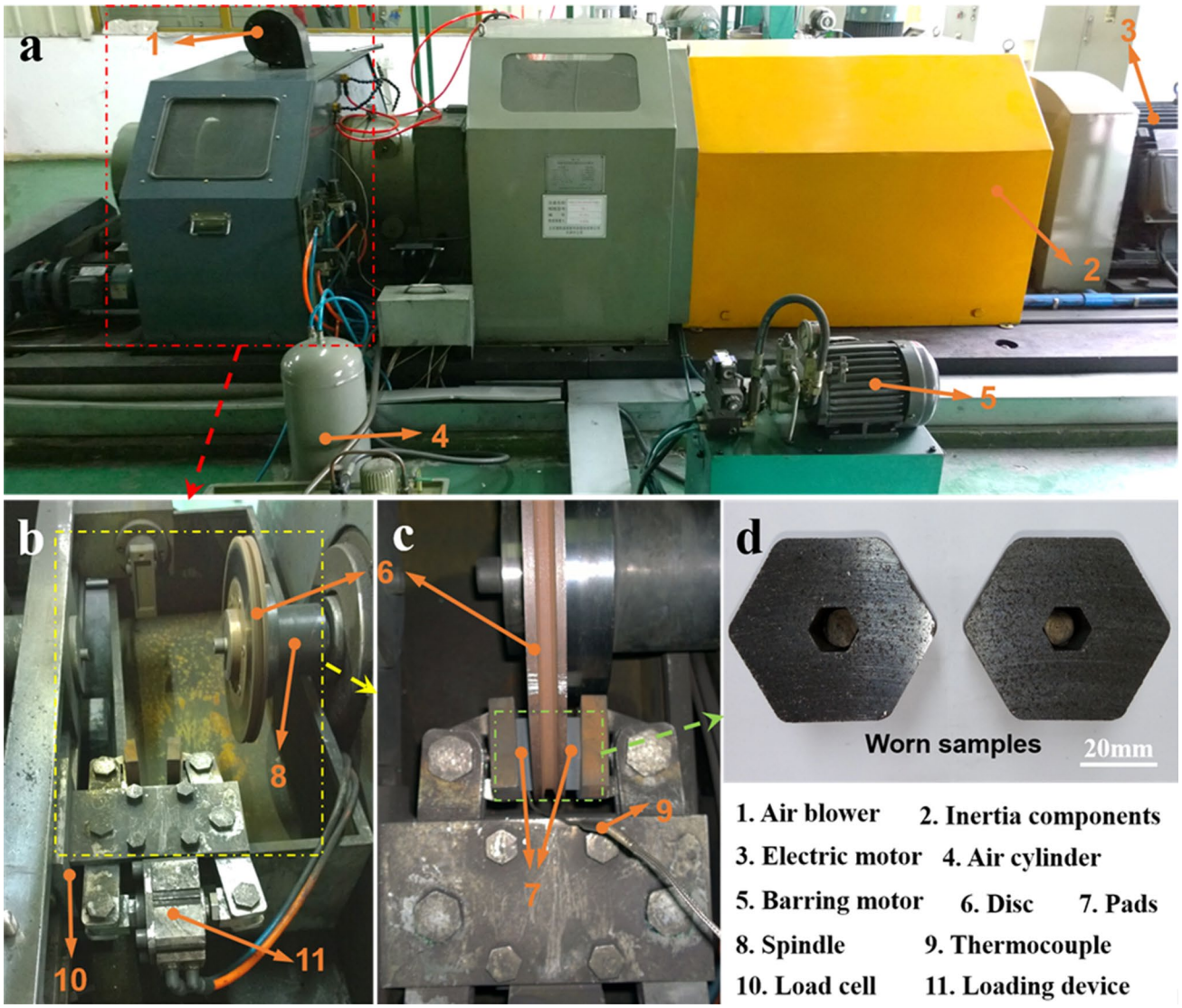

Fig. 2 Schematic diagram of the subscale brake testing apparatus. **a** External diagram, **b** inside diagram, **c** pad-on-disk configuration, **d** friction pads

Table 2 Physical and mechanical properties of the samples

Sample	Porosity (%)	Density (g/cm^3)	Brinell hardness (HB)	Shear strength (MPa)
S1	17.9	4.48	14.8	6.01
S2	18.1	4.44	15.4	7.03
S3	17.4	4.25	16.6	7.80
S4	18.4	4.16	22.4	10.71

3.2 Friction and Wear Behaviors of Different Samples

Figure 3 demonstrates the mean COF versus IBS curves at same pressure and inertia for different samples. Note that the mean COFs decreased with the increase in Fe content at any IBS. Another interesting phenomenon is turn point of mean COF–IBS curves with regard to Cu/Fe ratio: for the samples with Cu/Fe ratio > 1 (S1 and S2), the mean COF curves show a three-stage feature with rising IBS from 12 to 60 m/s, i.e., they firstly decreased with increasing IBS from 12 to 31 m/s, followed by an increase IBS from 31 to 47 m/s, and fell again with increasing IBS from 47 to 60 m/s. While for the samples with Cu/Fe ratio < 1 (S3 and S4), only

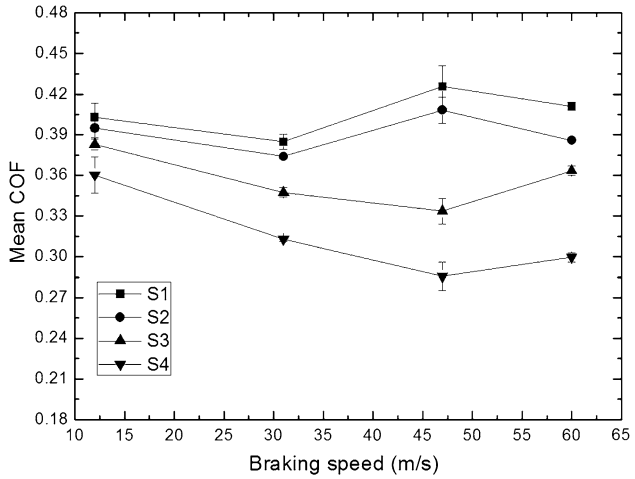

Fig. 3 Mean COF versus initial braking speed (IBS) for different samples

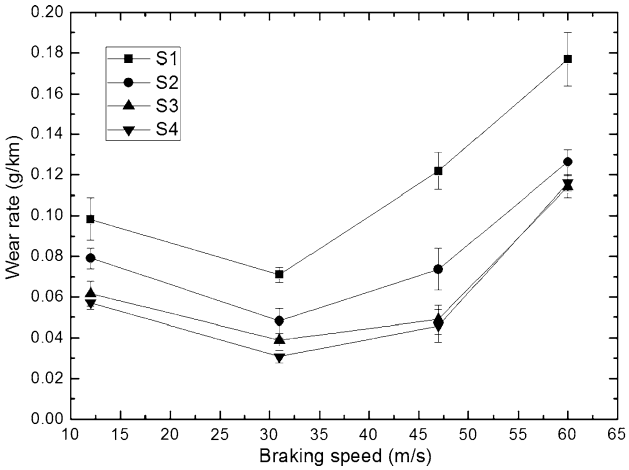

Fig. 5 Wear rate versus IBS for different samples

two-stage feature curves were found. That is, the mean COFs decreased with increasing IBS from 12 to 47 m/s, followed by a monotonic increase. At the transition point of 47 m/s, samples S1 and S2 reach the highest COF, but samples S3 and S4 display the lowest one.

Figure 4 shows the maximum subsurface temperatures (T_{max}) versus IBS. The T_{max} linearly increased with the IBS for all the samples. For a certain IBS, the T_{maxs} seemed closely for different samples, and it was hard to find out explicit relationships between the T_{max} and Fe content. Considering the measured T_{max} merely represented the bulk temperature 2 mm beneath the contact surface, the real temperature of contact sites must far above the value recorded.

The wear rates decreased with the increase in Fe content at any IBS, as shown in Fig. 5. Contrast to the changing rule

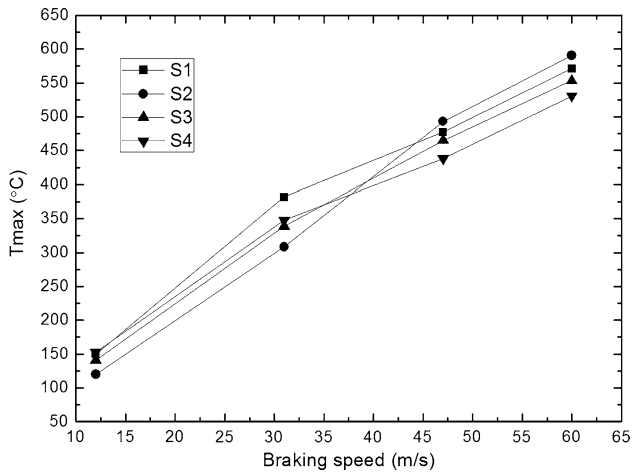

Fig. 4 Maximum subsurface temperatures (T_{max}) of the pad versus IBS for different samples

of mean COFs: when the Cu/Fe ratio > 1, the wear rates decreased remarkably as increasing iron content; when Cu/Fe ratio < 1, there was no distinct difference in wear rates. On the other hand, the wear rates were higher at both low IBS (12 m/s) and high IBS (60 m/s) but lower at medium IBS for all samples.

3.3 Morphologies of the Friction Surfaces

Figure 6 presents the representative morphologies of the friction surfaces. Note that the biggest difference between the surface morphologies of S1 and S4 is that the tribo-oxide film (in dark-gray contrast based on EDS identification) experienced distinct evolutions with IBS. Specifically, for S1, many hard particles (SiO_2) and graphite particles remained visible on the surface at 12 m/s (Fig. 6a), and a complete tribo-oxide film did not form until 31 m/s (Fig. 6b). When IBS reached 47 m/s, the tribo-oxide film began to rupture and the hard particles (SiO_2) and graphite resurfaced due to severe delamination wear (Fig. 6c), while these peeling pits seemed to be partly refilled by the wear debris at 60 m/s (Fig. 6d), and it may be caused by the excessive debris hard to be ejected from the tribological systems. However, for S4, the friction surface seemed smoother than that of S1 at 12 and 31 m/s due to the better coverage of tribo-oxide film (Fig. 6e, f). Besides, differed from S1, the tribo-oxide film of S4 seemed to experience re-compacted and still adhered to the surface at 47 m/s (Fig. 6g). And it is not until 60 m/s that the tribo-oxide film of S4 can be broken a lot on the surface (Fig. 6h).

On the other hand, the representative cross-sectional microstructures, as shown in Fig. 7, visually display the evolution of tribo-oxide film at different stage with regard to S1 and S4. For S1, the change in the cross-sectional microstructure is similar with our previous investigation [24]. At

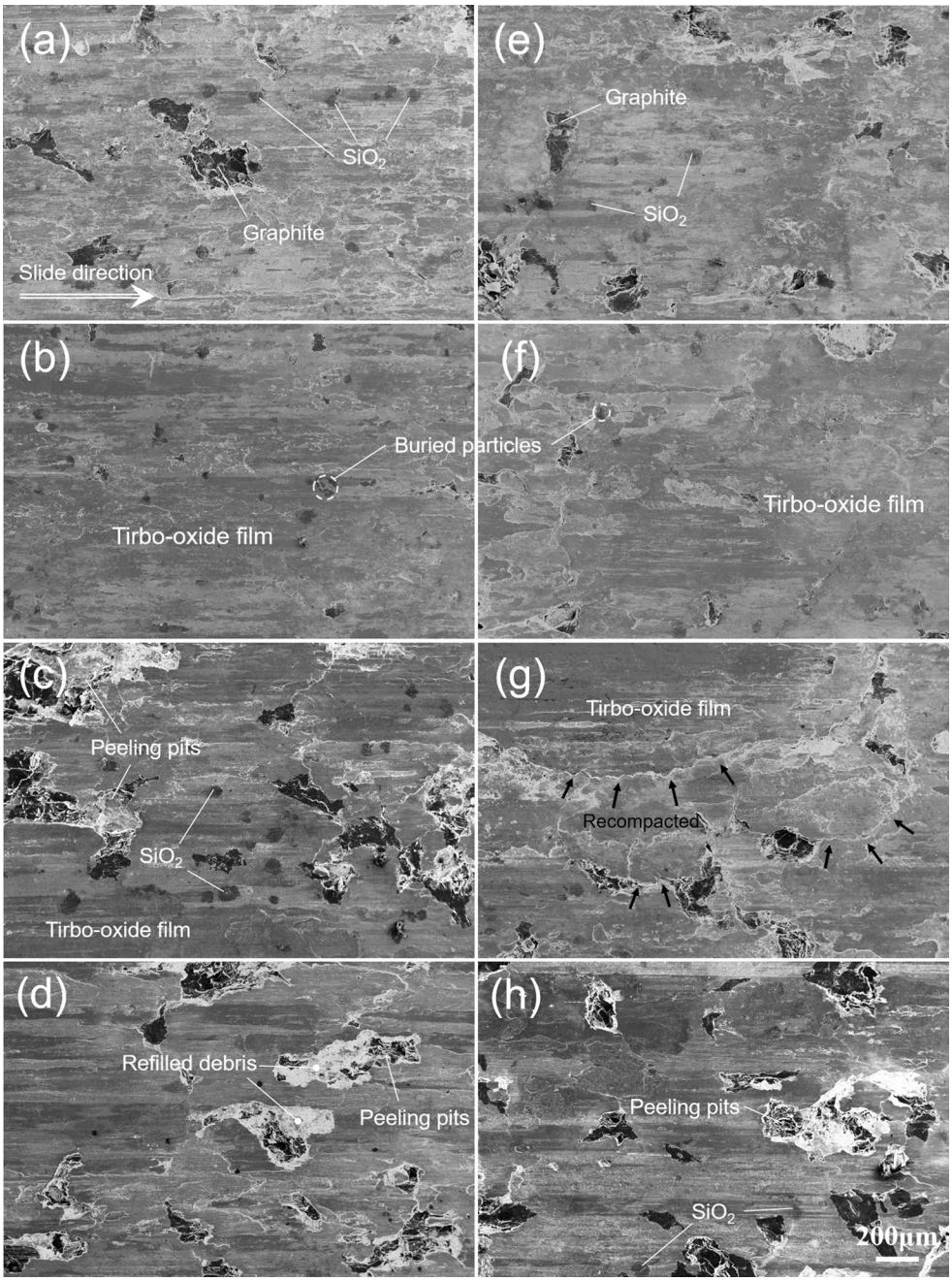

Fig. 6 Representative morphologies of the friction surfaces based on secondary electron image (SE). **a** S1, 12 m/s; **b** S1, 31 m/s; **c** S1, 47 m/s; **d** S1, 60 m/s; **e** S4, 12 m/s; **f** S4, 31 m/s; **g** S4, 47 m/s; **h** S4, 60 m/s. The bar scale is same for all the images

12 m/s, there was only a little film covering on the surface with the thickness of about 4 μm (Fig. 7a), and the complete tribo-oxide film (about 20 μm) did not form until 31 m/s (Fig. 7b). At 47 m/s, the tribo-oxide film was swept due to delamination (Fig. 7c). When IBS reached 60 m/s, a mass of wear debris was trapped to the existing potholes induced by delamination wear (Fig. 7d). There may be a tribo-sintering process for the trapped debris as found by Kato et al. [17], since this debris was still tightly bonded after ultrasonic cleaning in acetone before the SEM observation. For S4, the tribo-oxide film seems more adhesive than that of S1. There were also patches of film (about 6 μm) covering on the surface at 12 m/s (Fig. 7e), and the surface was fully covered by the complete tribo-oxide film (20–45 μm) at 31 m/s (Fig. 7f). When IBS increased to 47 m/s, different from S1, the tribo-oxide film of S4 grew thicker (38–50 μm) and still adhered to the substrate (Fig. 7g). When IBS reached 60 m/s, the tribo-oxide film began to rupture due to severe

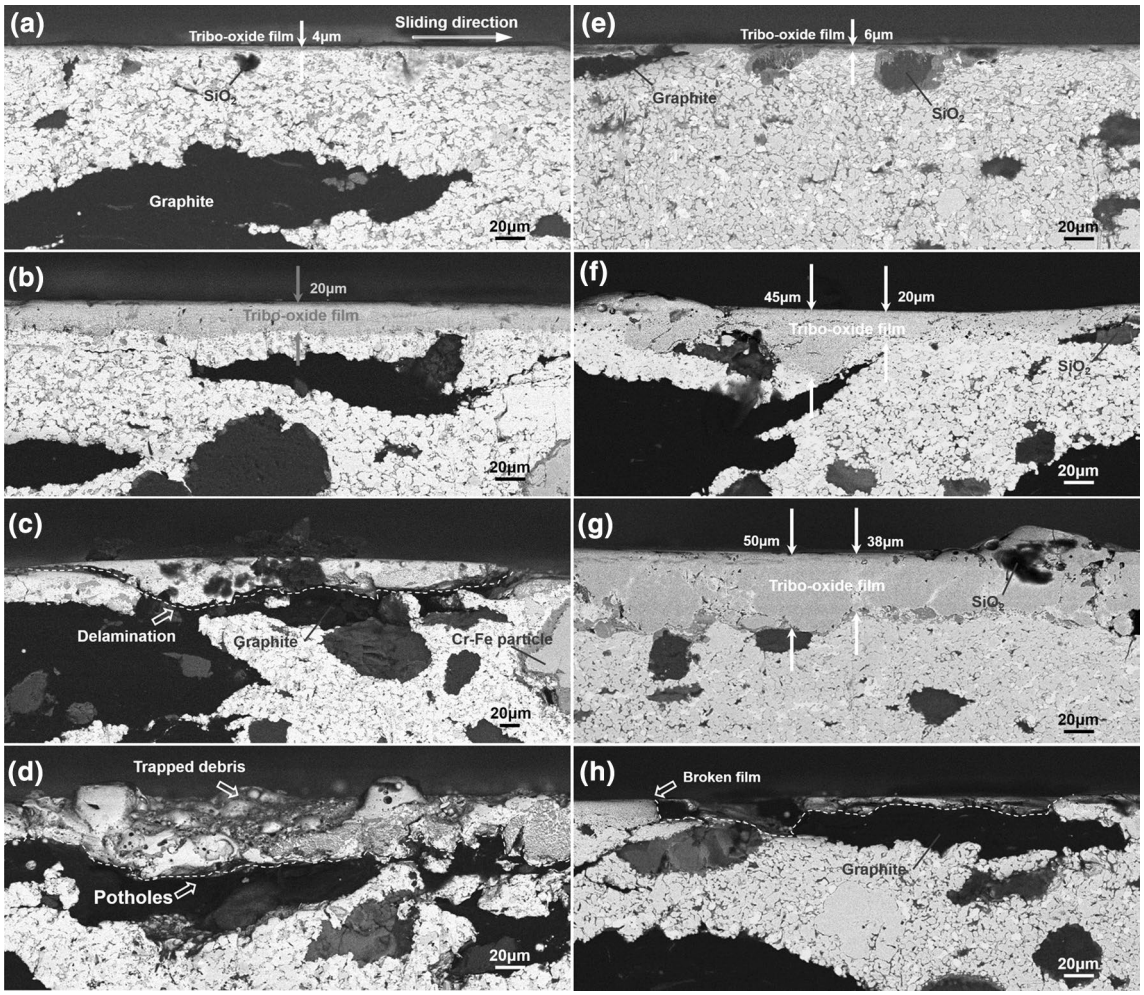

Fig. 7 Representative cross-sectional microstructures of the friction surface based on backscattered electron image (BSE). **a** S1, 12 m/s; **b** S1, 31 m/s; **c** S1, 47 m/s; **d** S1, 60 m/s; **e** S4, 12 m/s; **f** S4, 31 m/s; **g** S4, 47 m/s; **h** S4, 60 m/s

delamination (Fig. 7h). In general, the cross-sectional views indicate that the tribo-oxide film of S1 and S4 experienced different changes with IBS, which were compatible with the evolution of surface morphologies as mentioned above.

To further explore the compositional variation of friction surfaces under different IBS, XRD measurements were used and the representative patterns are shown in Fig. 8. It should be noted that the locations for main peak of Fe (110) at 2θ of 44.67° and Cr–Fe (110) at 2θ of 44.55° are overlapped and hard to be distinguished from each other in the XRD patterns. At low IBS (12 m/s), the oxide peaks, mainly Cu_2O and FeO, were very feeble in respect to S1 (Fig. 8a). This means that only a little oxides formed or remained under this IBS. As IBS increased, the intensity of FeO peak increased due to the oxidation of Fe, while the intensity of Cu_2O remained weak (Fig. 8a, b) due to low oxidation kinetics [16], and it will be discussed later. When IBS exceeded 47 m/s, the FeO was further oxidized to Fe_3O_4 and Fe_2O_3 (Fig. 8a, b). However, it is clearly observed that the relative intensity of oxides peaks (FeO, Fe_3O_4 and Fe_2O_3) in S1 was obviously inferior to that in S4 for any IBS (Fig. 8a, b), which was in conformity with the thickness of tribo-oxide film as shown in Fig. 7. On the other hand, the change in intensity of SiO_2 and graphite peaks for both S1 and S4 (Fig. 8a, b) seemed to accord with the formation and destruction of tribo-oxide film on the surfaces (Fig. 6), and it had been found in our previous work [24]. This means that the decrease in these peaks may be caused by the coverage of tribo-oxide film, while the re-growth of them probably induced by the peeling of the covered film.

3.4 Peeling Test of the Friction Surfaces

From above results, it seems that the higher the Fe content for the sample, the better the coverage tribo-oxide film on the surface (Figs. 6, 7), and the higher the critical IBS for the destruction of tribo-oxide film. To further ravel out the relationship between Cu/Fe ratio and the destruction

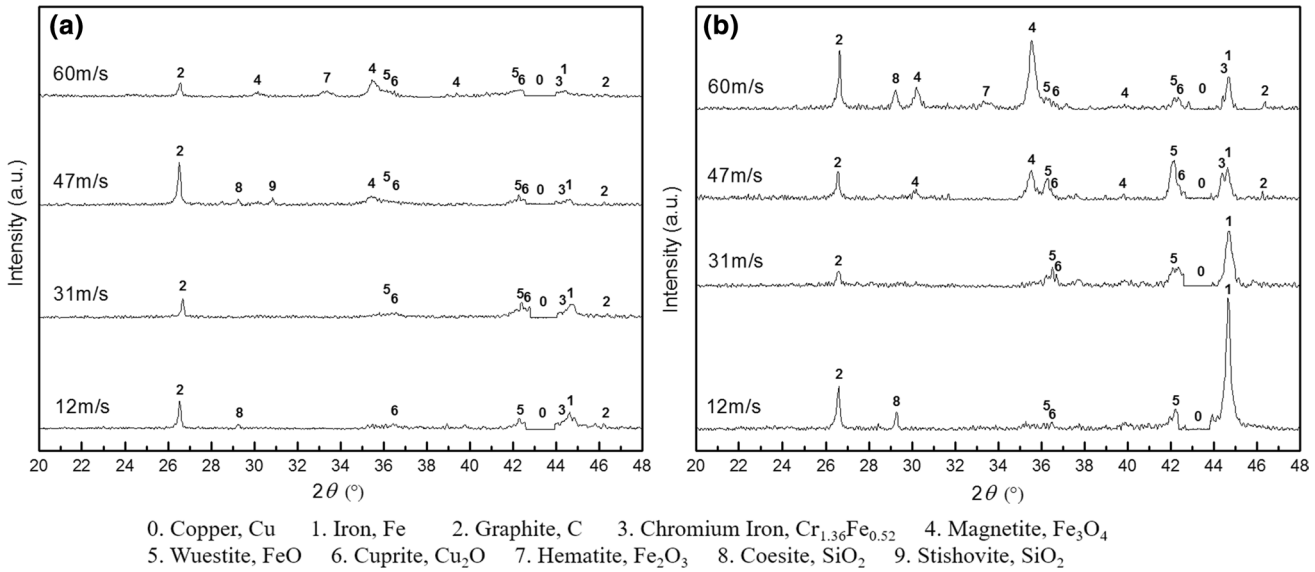

Fig. 8 Representative XRD patterns of the friction surfaces, **a** S1, **b** S4. Cu peak (marked "0") is too intensive and have been "cut off" from the patterns to allow "raising" the intensity of weaker peaks, and the intensively Cu and Fe peaks may be attributed to the penetration of tribo-film by X-ray

of tribo-oxide film, a pull-up peeling test involving epoxy bonding a 6-mm diameter stud to the friction surface was conducted on different samples. Since the destruction of tribo-oxide film results from the crack initiation and propagation in nature, it may be occurred either inside the tribo-oxide film or within the weakest interface of the composite, i.e., graphite/metals interface, the fracture strength of tribo-oxide film herewith can be characterized by the load required to cause failure of the friction surface due to their analogous process. To ensure the measured value was not entirely the fracture strength of composite, a contrast experiment was also applied to the initial surface (the initial surface was polished to #400 by silicon carbide abrasive paper, washed with acetone and dried prior to testing). The schematic diagram of the sample preparation and peeling test experiment is shown in Fig. 9. More details of this method can be found in the publications by Hou et al. [27] or by Wu et al. [28]. Fracture strength is taken to be the force required to pull the film from the substrate divided by the area of the loading pin. Three tested blocks took from the same sample were applied to the peeling tests, and the mean value (fracture strength) is reported in this work. It should be noted that failures occasionally occurred in the combinations of the film/substrate interface or the substrate, but barely occurred within the epoxy resin. What is more, two more adhesives were used to conduct the test, and the results were almost the same, which indicates that the strength of the tribo-oxide film was not affected by the resin in the peeling test. The pulled surface was then examined by SEM.

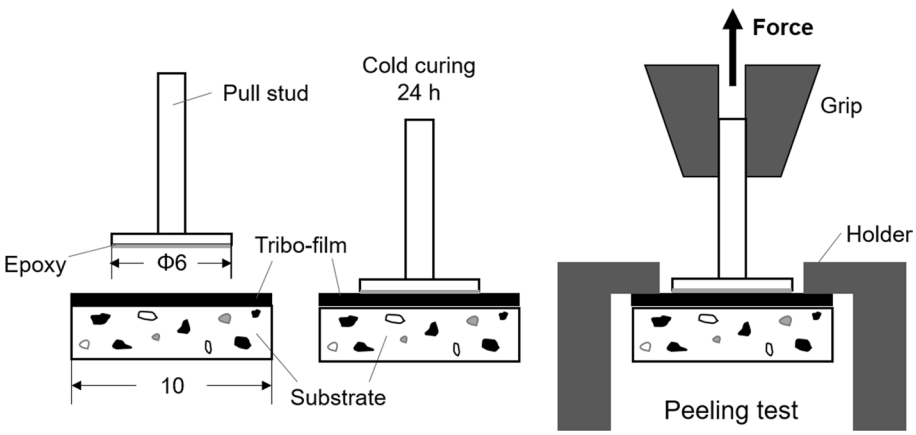

Fig. 9 Schematic presentation of the sample preparation for pull-up peeling test of tribo-oxide film

Table 3 Fracture strength (MPa) of the initial surface and the friction surface of different samples with IBS of 31 and 60 m/s

Sample	S1	S2	S3	S4
Initial surface	3.22 ± 0.21	3.86 ± 0.16	5.22 ± 0.32	5.76 ± 0.25
After 31 m/s	5.23 ± 0.54	5.91 ± 0.77	7.13 ± 1.30	9.58 ± 0.63
After 60 m/s	2.90 ± 0.64	3.36 ± 0.35	3.82 ± 1.43	5.06 ± 0.92

Table 3 lists the fracture strength of the initial surface and the friction surface of different samples. It can be seen that the fracture strength increased with the increase in Fe content no matter for the initial surface or for the friction surface. What is more, for each sample, the friction surface after IBS of 31 m/s displayed highest fracture strength among the three tested surfaces, followed by the initial surface, the friction surface after IBS of 60 m/s displayed a lowest one.

Figure 10 shows the representative morphologies of the pulled initial and friction surfaces as well as the corresponding elements (Cu, Fe, O, and C) area profiles after peeling test. Note that numerous graphite particles distributed on the fracture surface of initial sample (Fig. 10a). The bottom left inset in Fig. 10a shows

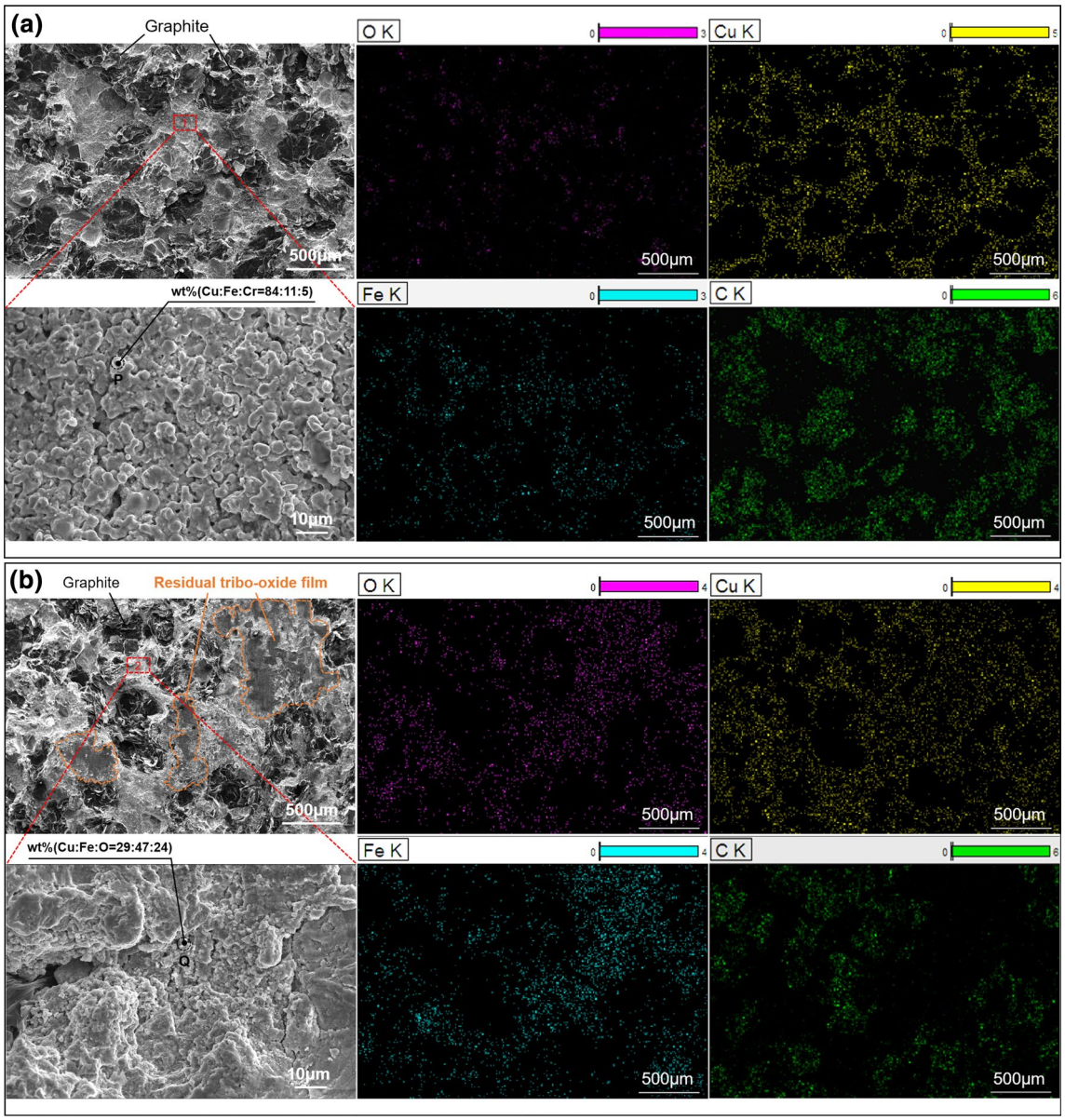

Fig. 10 Representative morphologies of **a** the initial surface of S2 after peeling test and the corresponding elements (Cu, Fe, O, and C) area profiles; the bottom left inset shows the fracture zone of the box "1". **b** The friction surface of S2 (31 m/s) after peeling test and the corresponding elements (Cu, Fe, O, and C) area profiles; the bottom left inset shows the fracture zone of the box "2"

a high-magnification micrograph of the marked fracture zone (box "1"). The corresponding chemical composition in point "P" (wt%-Cu/Fe/Cr = 84:11:5) suggests that this fracture zone (box "1") was metal matrix. This area was polyporous and without distinct dimple. These features indicate that the fracture mode was brittle failure in respect to the initial surface and the debonding preferentially occurred at the graphite/metals interface due to their weakest binding force. Similarly, the fractured friction surface (after 31 m/s) also presented many graphite particles (Fig. 10b). Besides, the element area profiles reveal that iron and oxygen showed marked enrichment at some irregular regions (marked by orange dashed line), indicating that there still was a portion of residual tribo-oxide film on the fracture surface. The bottom left inset in Fig. 10b shows a high-magnification micrograph of the marked fracture zone (box "2"). The shiny particles within the fracture zone (box "2") were identified to be composed of oxides (wt%-Cu/Fe/O = 29:47:24 in point "Q") based on EDS and the neck between the fine particles (~ 3 μm) was obviously visible, which featured an initial stage of sintering. (Figure 10b). Such findings indicate that the debonding mainly occurred at the graphite/metals interface and inside the tribo-oxide film.

Generally, the initial surface was expected to show the highest fracture strength compared to the friction surface, but that is not what happened. According to the fracture morphologies (Fig. 10a), the initial surface displayed brittle failure due to non-densification and the weak-bonding interface between graphite and metal, which resulting in the relative low fracture strength (Table 3). When the composite is subjected to high-speed and high-pressure friction, there may be deformation or micro-cracks within the surface and subsurface, which will reduce the mechanical properties. Nevertheless, there are also some other effects introduced by friction process. Adachi et al. [29] have experimentally proposed the possibility of tribo-sintering of fine alumina particles at the contact interface during friction under high pressure and high temperature. Kato et al. have shown clear evidence for the tribo-sintering of the supplied particles on the rubbing surfaces [17, 30], and claimed that formation of a wear-protective tribo-film on the surface is due to the tribo-sintering of wear particles. Therefore, the fracture strength of friction surface is influenced by both wear damage and tribo-sintering. In this experiment, for the specimens tested at IBS of 31 m/s, the tribo-oxides were solidly sintered together as shown in the bottom left inset in Fig. 10b, the tribo-sintering of tribo-oxides thereby may be intense while the wear damage within the subsurface may be relatively slight, which may be responsible for their higher resistance to peeling (Table 3). However, when the sliding speed is extremely high (60 m/s), wear damage became quite serious and there were numerous cracks in the surface and subsurface (Figs. 6d, h, 7d, h), which caused the lowest fracture strength in respect to the friction surfaces after IBS of 60 m/s (Table 3). Such findings suggest that the moderate friction contributes to form a protective tribo-oxide film on the surface while the excessive friction leads to the deterioration of contact surface.

4 Discussion

From the above-mentioned description, we have found that, for a certain IBS, both the mean COFs and wear rates decreased with the increase in Fe content. Such findings were distinct from the previous study [6], in which the friction coefficient increased with the increase in Fe content from 0 to 12 wt%. Perhaps because of the mild sliding conditions (lower applied pressure of 0.5 MPa, lower sliding speeds of 3–24 m/s, and very low rotary inertia of 0.245 kg m^2) they used for testing, they only attributed that result to the properties of Fe itself. As introduced in the opening part, the tribo-oxidation generally is inevitable under realistic braking. Thus, the metals may exist in the form of metallic oxides on the friction surface, such as FeO, Fe_3O_4, Fe_2O_3, Cu_2O, and CuO in our experiments (Fig. 8). These oxides usually occupied the main part of the tribo-oxide film, which were frequently reported in the literatures [15, 31–33]. In this case, the tribological behaviors of the samples should be more correlated with the formed tribo-oxide film on the friction surface than metals themselves. In order to fully illustrate the relevance between Cu/Fe ratio

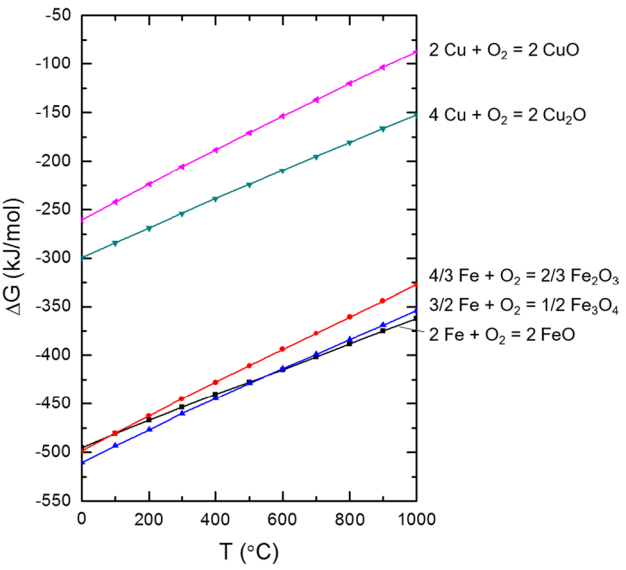

Fig. 11 Simplified Ellingham diagram indicating the relative free energies for various metal oxidation reactions [16]

and the tribo-oxide film as well as the mean COF and wear rate behaviors, we make the following analyses.

It is known that iron oxides (FeO, Fe_3O_4 and Fe_2O_3) are highly stable relative to cupric oxides (Cu_2O and CuO) based on Ellingham diagram (Fig. 11) [16]. The tribo-oxide film would be more easily to form on the friction surface with regard to the sample containing more Fe due to higher oxidation kinetics of Fe. As a consequence, the higher the Fe content for the brake pad under braking, the better the coverage of tribo-oxide film on the surface, as shown in Figs. 6 and 7. Since tribo-oxide film can effectively prevent metal-on-metal contact [19–23] (commonly relates to adhesion and large volume of plastic deformation, which is considered to be the primary course of energy dissipation during friction [34], i.e., the major term of friction force), as well as protect the substrate from being destructed as interpreted in Sect. 3.4. The increase in Fe content could thereby contribute to the decrease in mean COF and wear rate in respect to brake materials. In addition, the effect of tribo-oxide film on the tribological behaviors also can be indirectly illustrated by the following facts. When the tribo-oxide film was nearly non-formation or less-formation due to lacking thermal activation at low IBS of 12 m/s (Figs. 6a, e, 7a, e), the mean COFs of different samples were close at this time (Fig. 4). As IBS increased, the coverage of tribo-oxide film grew faster in respect to the sample containing more Fe (Figs. 6b, f, g, 7b, f, g) and the gap of mean COFs between different samples expanded gradually before 47 m/s (Fig. 4). Beyond 47 m/s, the transition of mean COFs were associated with the destruction of tribo-oxide film (Figs. 6c, d, h, 7c, d, h). However, the similar wear rates in respect to the samples with Cu/Fe ratio < 1 (Fig. 5) may be because the formed tribo-oxide film reached the tolerance limit for the surface.

Other remarkable findings are that there were some transition points in the mean COFs and wear rates curves with regard to all the samples. As IBS exceeded these points, i.e., critical IBS, the mean COFs began to increase and the wear rates began to sharply increase with increasing IBS (Figs. 4, 5). Meanwhile, there were also some other critical IBSs corresponding to the destruction of tribo-oxide film on the surface (Figs. 6c, h, 7c, h). It is noteworthy that the critical IBS for the transition of mean COFs and wear rates in respect to the sample with Cu/Fe ratio < 1 (at IBS of 47 m/s) basically lagged behind that in the sample with Cu/Fe ratio > 1 (at IBS of 31 m/s). Not surprisingly, this result is coincident with the behavior of critical IBS for the destruction of tribo-oxide film on the surface in respect to different samples, i.e., the sample with higher Fe content showed a higher critical IBS for the destruction of tribo-oxide film than the sample with lower Fe content (Figs. 6c, h, 7c, h). Such phenomena may be attributed to the inhibition effect of Fe on the destruction of tribo-oxide film. As mentioned in Sect. 3.4, the fracture strength of tribo-oxide film increased with the increase in Fe content no matter for the friction surface or for the initial surface. It indicates that the higher the Fe content for the sample, the harder the destruction of tribo-oxide film on the surface. Since the debonding preferentially occurred inside the tribo-oxide film and at the graphite/metals interface (Fig. 10), the destruction of tribo-oxide film is correlated with the cohesion of tribo-oxides themselves (or the adhesion of tribo-oxides/substrate) and the bonding strength of the graphite/metals interface. There is no doubt that the higher the Fe content, the more iron oxides (FeO, Fe_3O_4 and Fe_2O_3) the tribo-oxide film contains, and the fewer the copper oxides (CuO_2). Note that the ratio of the thermal expansion coefficient of Fe to that for FeO, Fe_3O_4 and Fe_2O_3 is 1.25, 1.46, and 1.39 [35], respectively, which is far below that value for Cu to Cu_2O (4.3) [36]. Therefore, the tribo-oxide film containing more iron oxides may adhere tighter to the substrate due to less thermal stress (tensile stress) induced by the friction heat during braking. What is more, since the wettability between Fe and graphite is better than that between Cu and graphite (neither mutual dissolution, nor to form a stable carbide), the bonding strength of Fe/graphite interface may be higher than that of Cu/graphite interface, which may be also responsible for the increased resistance to peeling with increasing Fe content.

Based on above analyses, the mean COFs and wear rates decreased with the increase in Fe content for a certain IBS can be attributed to the easier formation and harder destruction of tribo-oxide film on the surface in respect to the sample containing more Fe. Besides, the higher the Fe content for the sample, the higher the critical IBS for the destruction of tribo-oxide film on the surface, and the higher the critical IBS for the transition of mean COF and wear rate.

5 Conclusions

1. Different from the previous studies, in our work, the brake friction composite containing more Fe content always showed lower mean COF and wear rate.
2. The tribological behavior of composite at different IBS depends not just on the formation of tribo-oxide film, but on the destruction of tribo-oxide film.
3. Higher Fe content accelerated the formation of tribo-oxide film and in turn inhibited the destruction of tribo-oxide film on the surface, leading to lower mean COF and wear rate, as well as a higher critical IBS for the transition of mean COF and wear rate.
4. The fracture strength of the tribo-oxide film can be characterized by the peeling test. The tests also show that the

moderate friction contributes to form a protective tribo-oxide film on the surface due to tribo-sintering effect while the excessive friction leads to the deterioration of composite.

Acknowledgements Financial support from the National Natural Science Foundation of China under Contract No. 51572026 is gratefully acknowledged.

References

1. Kang, S.: A study of friction and wear characteristics of copper- and iron-based sintered materials. Wear **162–164**, 1123 (1993)
2. Su, L., Gao, F., Han, X., Fu, R., Zhang, E.: Tribological behavior of copper–graphite powder third body on copper-based friction materials. Tribol. Lett. **60**, 30 (2015)
3. Prabhu, T.R., Varma, V.K., Vedantam, S.: Effect of reinforcement type, size, and volume fraction on the tribological behavior of Fe matrix composites at high sliding speed conditions. Wear **309**, 247 (2014)
4. Li, G., Yan, Q.: Comparison of friction and wear behavior between C/C, C/C-SiC and metallic composite materials. Tribol. Lett. **60**, 15 (2015)
5. Yun, R., Filip, P., Lu, Y.: Performance and evaluation of eco-friendly brake friction materials. Tribol. Int. **43**, 2010 (2010)
6. Xiong, X., Chen, J., Yao, P., Li, S., Huang, B.: Friction and wear behaviors and mechanisms of Fe and SiO_2 in Cu-based P/M friction materials. Wear **262**, 1182 (2007)
7. Chen, B., Bi, Q., Yang, J., Xia, Y., Hao, J.: Tribological properties of solid lubricants (graphite, h-BN) for Cu-based P/M friction composites. Tribol. Int. **41**, 1145 (2008)
8. Winkelmann, H., Varga, M., Badisch, E.: Influence of secondary precipitations in Fe-based mmcs on high temperature wear behaviour. Tribol. Lett. **43**, 229 (2011)
9. Cui, G., Lu, L., Wu, J., Liu, Y., Gao, G.: Microstructure and tribological properties of Fe–Cr matrix self-lubricating composites against Si_3N_4 at high temperature. J. Alloys Compd. **611**, 235 (2014)
10. Jang, H., Ko, K., Kim, S.J., Basch, R.H., Fash, J.W.: The effect of metal fibers on the friction performance of automotive brake friction materials. Wear **256**, 406 (2004)
11. Su, L., Gao, F., Han, X., Chen, J.: Effect of copper powder third body on tribological property of copper-based friction materials. Tribol. Int. **90**, 420 (2015)
12. Li, J., Yin, Y., Ma, H.: Preparation and properties of Fe_3Al-based friction materials. Tribol. Int. **38**, 159 (2005)
13. Verma, P.C., Ciudin, R., Bonfanti, A., Aswath, P., Straffelini, G., Gialanella, S.: Role of the friction layer in the high-temperature pin-on-disc study of a brake material. Wear **346–347**, 56 (2016)
14. Tjong, S.C., Lau, K.C.: Tribological behaviour of SiC particle–reinforced copper matrix composites. Mater. Lett. **43**, 274 (2000)
15. Österle, W., Urban, I.: Friction layers and friction films on PMC brake pads. Wear **257**, 215 (2004)
16. Blau, P.J.: Elevated-temperature tribology of metallic materials. Tribol. Int. **43**, 1203 (2010)
17. Kato, H., Komai, K.: Tribofilm formation and mild wear by tribo-sintering of nanometer-sized oxide particles on rubbing steel surfaces. Wear **262**, 36 (2007)
18. Jiang, J., Stott, F.H., Stack, M.M.: The role of triboparticles in dry sliding wear. Tribol. Int. **31**, 245 (1998)
19. Godet, M.: The third-body approach: a mechanical view of wear. Wear **100**, 437 (1984)
20. Desplanques, Y., Degallaix, G.: Genesis of the third-body at the pad-disc interface: case study of sintered metal matrix composite lining material. SAE Int. J. Mater. Manuf. **2**, 25 (2010)
21. Haddad, H., Guessasma, M., Fortin, J.: A DEM–FEM coupling based approach simulating thermomechanical behaviour of frictional bodies with interface layer. Int. J. Solids Struct. **81**, 203 (2016)
22. Jacko, M.G., Tsang, P.H.S., Rhee, S.K.: Wear debris compaction and friction film formation of polymer composites. Wear **133**, 23 (1989)
23. Österle, W., Dörfel, I., Prietzel, C., Rooch, H., Cristol-Bulthé, A.L., Degallaix, G., Desplanques, Y.: A comprehensive microscopic study of third body formation at the interface between a brake pad and brake disc during the final stage of a pin-on-disc test. Wear **267**, 781 (2009)
24. Peng, T., Yan, Q., Li, G., Zhang, X., Wen, Z., Jin, X.: The braking behaviors of Cu-based metallic brake pad for high-speed train under different initial braking speed. Tribol. Lett. (2017). https://doi.org/10.1007/s11249-017-0914-9
25. Huang, Z., Zhai, H., Guan, M., Liu, X., Ai, M., Zhou, Y.: Oxide-film-dependent tribological behaviors of Ti_3SiC_2. Wear **262**, 1079 (2007)
26. Desplanques, Y., Degallaix, G.: Interactions between third-body flows and localisation phenomena during railway high-energy stop braking. SAE Int. J. Passeng. Cars Mech. Syst. **1**, 1267 (2008)
27. Hou, P.Y., Priimak, K.: Interfacial segregation, pore formation, and scale adhesion on NiAl alloys. Oxid. Met. **63**, 113 (2005)
28. Wu, T., Tong, J., Hsieh, J.J., Yang, Y.S.: Improvement of interfacial adhesion of Al/Cr films deposited on indium tin oxide coated glasses by interfacial oxidation. Surf. Coat. Technol. **183**, 89 (2004)
29. Adachi, K., Koji, K.: Formation of smooth wear surfaces on alumina ceramics by embedding and tribo-sintering of fine wear particles. Wear **245**, 84 (2000)
30. Kato, H.: Effects of supply of fine oxide particles onto rubbing steel surfaces on severe-mild wear transition and oxide film formation. Tribol. Int. **41**, 735 (2008)
31. Quinn, T., Sullivan, J., Rowson, M.: Origins and development of oxidational wear at low ambient temperatures. Wear **94**, 175 (1984)
32. So, H., Yu, D.S., Chuang, C.Y.: Formation and wear mechanism of tribo-oxides and the regime of oxidational wear of steel. Wear **253**, 1004 (2002)
33. Garbar, I.I.: Gradation of oxidational wear of metals. Tribol. Int. **35**, 749 (2002)
34. Rigney, D.A., Hirth, J.P.: Plastic deformation and sliding friction of metals. Wear **53**, 345 (1979)
35. Mcneill, L.S., Edwards, M.: The importance of temperature in assessing iron pipe corrosion in water distribution systems. Environ. Monit. Assess. **77**, 229 (2002)
36. Rakhshani, A.E.: Preparation, Characteristics and photovoltaic properties of cuprous oxide—a review. Solid State Electron. **29**, 7 (1986)